

# Unified dynamic approach for simulating quantum tunneling and thermionic emission at metal/organic interface

Jiaqing Huang, Yijie Mo, and Yao Yao\*

*Department of Physics and State Key Laboratory of Luminescent Materials and Devices,  
South China University of Technology, Guangzhou 510640, China*

## Abstract

Injection from metallic electrodes serves as a main channel of charge generation in organic semiconducting devices and the quantum effect is normally regarded to be essential. We develop a dynamic approach based upon the surface hopping (SH) algorithm and classical device modeling, by which both quantum tunneling and thermionic emission of charge carrier injection at metal/organic interfaces are concurrently investigated. The injected charges from metallic electrode are observed to quickly spread onto the organic molecules following by an accumulation close to the interface induced by the built-in electric field, exhibiting a transition from delocalization to localization. We compare the Ehrenfest dynamics on mean-field level and the SH algorithm by simulating the temperature dependence of charge injection dynamics, and it is found that the former one leads to an improper result that the injection efficiency decreases with increasing temperature at room-temperature regime while SH results are credible. The relationship between injected charges and the applied bias voltage suggests it is the quantum tunneling that dominates the low-threshold injection characteristics in molecular crystals, which is further supported by the calculation results of small entropy change during the injection processes. An optimum interfacial width for charge injection efficiency at the interface is also quantified and can be utilized to understand the role of interfacial buffer layer in practical devices.

---

\*Electronic address: yaoyao2016@scut.edu.cn

## I. INTRODUCTION

The successful industrial application of organic light emitting device (OLED) might be one of the great scientific achievements in the last decades. Researchers are still devoting effort to improve the efficiency so that it can be extended to more application scenarios such as illumination, and more comprehensive analysis of the microscopic working mechanism is thus highly demanded [1–5]. Due to the cost control, the organic semiconductors are normally in amorphous phase and the contacts between conducting layer and electrodes are regarded to be poor. Moreover, different from the inorganic semiconductors in which intentional doping gives rise to numerous charge carriers, the main source of carriers in organic semiconductors stems from metallic electrodes. Therefore, the injection efficiency at the metal/organic interfaces has a significant impact on the overall performance of organic semiconducting devices.

In statistical physics, the charge injection at interfaces can be well described by the Richardson formula in the framework of thermionic emission theory [6]. This theory is valid when the concentration of doped charges in inorganic semiconductors is sufficiently large so that the injected carriers would not drive the system far away from thermal equilibrium and the detailed balance principle matters. In this perspective, giving the structure of single-electron energy spectrum it is able to derive the injected current and the details of dynamical processes are not important. On the experimental side, therefore, the techniques such as the ultraviolet photoelectron spectroscopy are widely used to study the energy level alignment at these interfaces and thus the magnitude of the barrier for charge injection can be determined [7–10]. In contrast to the inorganic semiconductors, the charge injection at the metal/organic interfaces dominates the generation and interfacial recombination of charge carriers. Either thermionic emission or quantum tunneling may play the key role in the charge injection. Since the semiconductors are almost without free charges in the initial (as-prepared) stage, the injected charge easily enforces the system to the nonequilibrium state and the dynamical process of injection turns out to be essential. In addition, organic materials normally possess strong electron-phonon interactions, making the intrinsic mechanisms of charge injection more complicated [11].

In recent years, mixed quantum-classical dynamics (MQCD) has become an important tool to study the charge injection and transport properties in the organic semiconductors

[12–22]. The MQCD can be generally performed in two different ways: The Ehrenfest dynamics and the surface hopping (SH) algorithm. The Ehrenfest dynamics based on the mean-field theory has a simple formulation in which the mean trajectory evolves on an effective potential energy surface (PES) for the electronic states and has been applied to the charge injection in the organic semiconductors by several groups [23–27]. By simulating the electron injection in a metal/polymer/metal structure, Wu and co-workers found that the injection of electron finally led to the formation of polaron or bipolaron and the electric field applied on the polymer could effectively reduce the interfacial potential barrier for charge injection from metallic electrode to polymer [23, 24]. Similarly, Johansson and Stafström simulated the formation of polaron in an isolated polymer chain [25], while Fu and co-workers considered the similar issue in a metal/polymer structure [26]. More recently, Ribeiro Junior and da Cunha obtained the polaron-type products through the careful investigations of the hole injection dynamics in polymers [27]. In these works, the Ehrenfest dynamics were performed in the framework of the tight-binding Su-Schrieffer-Heeger model to describe the dynamic properties of the charge injection process. Although it works well for the simulation of elementary quasi-particles, it merely takes one effective PES into account and is not satisfactory when there is a large barrier and the quantum tunneling is remarkable. The discussion of charge injection in the practical organic semiconductors is still one of the pronounced topics especially when the device physicists want to understand the role of realistic device parameters such as the electric field, the interfacial morphology and so on.

It is known that due to the strong interaction between electrons and phonons, the organic systems may undergo non-adiabatic transitions among different PESs. The non-adiabatic phenomena are very common for a large number of situations, such as the atomic and molecular collision reactions, molecular photochemistry and photophysics, and photoexcitation of condensed phase systems [17, 18]. In recent years, the SH algorithm has become a crucial tool for the dynamic propagation of non-adiabatic systems in physics, chemistry and material sciences [17–22]. In this algorithm, the nuclei move on an active PES with respect to the classical Newton equation and behave stochastic hops among different PESs based on the population flux among adiabatic electronic states. Tully’s standard fewest switches surface hopping and its developed algorithms have been successfully used to study the charge transport in molecular crystals and the results always enlighten the importance of non-adiabatic transitions or quantum tunnelings for organic semiconductors [28–35]. The present work

is thus motivated to provide a unified approach based on the SH algorithm to simulate the charge injection process for different situations, no matter the quantum tunneling or thermionic emission dominates.

As typical organic semiconducting materials, the rubrene possesses large mobility and has lately attracted much research interest due to its low-threshold injection characteristics in heterojunction devices [36–40]. In this work, by embedding the classical Poisson’s equation into the standard SH algorithm, the non-adiabatic dynamics of the charge injection at the metal/organic interfaces is investigated within the framework of a molecular crystal model. The generation of the injected charges will be firstly discussed. The injected charges calculated by the SH algorithm will be compared with the results by the Ehrenfest dynamics. The influence of the bias voltage applied at the metallic electrode on the injected charges and the optimum width of the interfacial layer for the charge injection will be investigated. Finally, the charge injection process at the metal/organic interfaces will be featured by the evolution of entropy change. The paper is organized in the following sequence. The model for the metal/organic system and the dynamic evolution method are given in Section II. The results and discussion are presented in Section III. Finally, in Section IV, the main conclusions are drawn.

## II. MODEL AND METHOD

Throughout this work, we take rubrene as instance to show the simulation results from our developed dynamic approach. Without loss of generality, a metallic electrode and the rubrene molecules are placed head-to-tail to construct a one-dimensional metal/organic structure, in which totally 160 sites are considered and we take 70 sites on the left to mimic the atoms of metallic electrode and the other 90 sites on the right for the organic molecules, respectively. Moreover, as a crucial consideration of this work, we notice that the morphology of the interface is essential for the charge injection. Specifically, as the organic materials are normally soft and amorphous, there is remarkable permeability of organic molecules into the metallic electrode. Therefore, a certain number of sites in the electrode close to the organic side will be regarded as the interfacial layer.

The model Hamiltonian consists of three terms as follows:

$$H = H_{\text{ele}} + H_{\text{lat}} + H_{\text{ext}}. \quad (1)$$

The first term in Eq. (1) is the electronic Hamiltonian expressed as

$$H_{\text{ele}} = - \sum_n t_n (\hat{c}_{n+1}^\dagger \hat{c}_n + \text{h.c.}), \quad (2)$$

where  $\hat{c}_n^\dagger$  ( $\hat{c}_n$ ) creates (annihilates) an electron on  $n$ -th site and  $t_n = t_{0(1)} - \alpha_n(u_{n+1} - u_n)$  is the nearest-neighbor hopping integral in which the vibronic coupling is involved, namely, with  $\alpha_n$  being the vibronic coupling strength and  $u_n$  being the displacement of  $n$ -th site. Herein,  $t_0$  is the hopping constant in both electrode and organic material, and  $t_1$  is the coupling between them. The vibronic coupling  $\alpha_n = 0$  for metallic sites far away from interface so that it is gapless. For the organic molecules, we take uniform vibronic couplings, namely  $\alpha_n = \alpha$ , so that the initial state of the organic molecules is dimerized due to the Peierls instability and the gap is determined by the value of  $\alpha$ . In this situation, there naturally exists a barrier between electrode and organic material. In the interfacial layer, the vibronic coupling strength in the side of metallic electrode is given by a half Gaussian function, namely,

$$\alpha_n = \alpha \exp[-4(n - n_0)^2/W^2], \quad (3)$$

with  $n_0$  being the last site of the metallic electrode and  $W$  being the width of the interfacial layer. Here,  $W$  is an essential parameter in our model to characterize the interface.

The second term in Eq. (1) represents the elastic potential and kinetic energy of the molecules,

$$H_{\text{lat}} = \frac{K}{2} \sum_n (u_{n+1} - u_n)^2 + \frac{M}{2} \sum_n \dot{u}_n^2, \quad (4)$$

with  $K$  being the elastic constant and  $M$  being the mass of molecules.

The third term of Eq. (1) describes the contribution from the external field and has the following form

$$H_{\text{ext}} = \sum_n U_n(t) \hat{c}_n^\dagger \hat{c}_n, \quad (5)$$

where  $U_n(t)$  is the potential energy induced by the applied bias voltage and the electric field. In the metallic electrode a bias voltage is applied and written as  $U_n(t) = |e|V(t)$ . In the organic molecules an electric field  $E_n(t)$  along the  $-\hat{x}$  direction is thus generated and then the potential energy is determined by  $U_n(t) = -|e|V_n(t)$ . As another important input of our approach, we consider to embed the device modeling into the dynamic simulations. That is, considering the feedback of the distribution of the injected charges onto the electric field,

$E_n(t)$  and  $V_n(t)$  are given by the Poisson's equation [41–43]:

$$E_n(t) = E_{n-1}(t) - \frac{|e|a_0\rho_n(t)}{\varepsilon_r\varepsilon_0V_{\text{rub}}}, \quad V_n(t) = V_{n-1}(t) - E_n(t)a_0, \quad (6)$$

where  $e$  is the elementary charge of an electron,  $\varepsilon_r$  is the relative dielectric constant,  $\varepsilon_0$  is the permittivity of vacuum,  $a_0$  is the lattice constant,  $V_{\text{rub}}$  is the occupying volume of a single molecule and  $\rho_n$  is the injected charges on the  $n$ -th site. In the practical simulations, in order to minimize the numerical errors, we turned on the external field smoothly by using a half Gaussian function, that is,  $V(t) = V_0 \exp[-(t - t_c)^2/t_w^2]$  for  $0 < t < t_c$  and  $V(t) = V_0$  for  $t \geq t_c$  with  $t_c$  being a smooth turn-on period and  $t_w$  the width. We set  $t_c = 30$  fs and  $t_w = 25$  fs which are optimum values for numerical accuracy through our testing. The electric field  $E_1(t)$  at the first organic molecule is also turned on smoothly in the same way, and the initial value  $E_1$  is determined by  $V_0 = La_0E_1$  with  $L$  being the site number of the organic molecules.

The model parameters in this work are obtained from the earlier work by Troisi for investigating the charge transport of rubrene, namely,  $t_0 = 1150 \text{ cm}^{-1}$ ,  $\alpha = 3980 \text{ cm}^{-1}/\text{\AA}$ ,  $K = 48200 \text{ amu/ps}^2$ ,  $M = 532 \text{ amu}$  [13], and  $a_0 = 3.4 \text{ \AA}$ ,  $V_{\text{rub}} = 760 \text{ \AA}^3$  by our computations. For most organic materials, the dielectric constant normally ranges between 3 and 4 [44], and we set it to 4 in this work. For description of the metal/organic interface with a potential barrier, we set  $t_1 = 0.8t_0$ .

The motion of the sites can be described by the Newtonian equation. As we want to concurrently take the thermionic emission into account, the temperature should also be involved as a parameter in our model. Hence, the Langevin equation is employed as follows:

$$F_n(t) = M\ddot{u}_n = -K[2u_n - u_{n+1} - u_{n-1}] + \alpha_n[\rho_{n,n+1} - \rho_{n-1,n} + \rho_{n+1,n} - \rho_{n,n-1}] - \gamma M\dot{u}_n + \xi_n. \quad (7)$$

Herein,  $F_n(t)$  represents the force exerted on the  $n$ -th site and the density matrix  $\rho$  is given by  $\rho_{n,n'} = \sum_{\mu} \psi_{\mu,n}^*(t) f_{\mu} \psi_{\mu,n'}(t)$  with  $f_{\mu}$  (equals to 0, 1 or 2) being the time-independent distribution function determined by the initial occupation of electrons,  $\gamma$  is the friction coefficient which is set to  $0.01 \text{ ps}^{-1}$ , and  $\xi_n$  is a Markovian Gaussian random force with standard deviation  $(2\gamma Mk_B T/\Delta t)^{1/2}$  to mimic the thermal effect. With these considerations, the lattice displacement  $u_n(t_{j+1})$  and the velocity  $\dot{u}_n(t_{j+1})$  are respectively given by

$$u_n(t_{j+1}) = u_n(t_j) + \dot{u}_n(t_j)\Delta t, \quad \dot{u}_n(t_{j+1}) = \dot{u}_n(t_j) + \frac{F_n(t_j)}{M}\Delta t. \quad (8)$$

The time evolution of the electronic wavefunction is given by the time-dependent Schrödinger equation:

$$i\hbar \frac{\partial \psi_{\mu,n}(t)}{\partial t} = -t_n \psi_{\mu,n+1}(t) - t_{n-1} \psi_{\mu,n-1}(t), \quad (9)$$

where  $\psi_{\mu,n}$  is the  $\mu$ -th eigenstate of the Hamiltonian (1) on the  $n$ -th site. Herein, in order to numerically solve the electronic wavefunction, the integration time step  $\Delta t$  in the discretization procedure must be set to be sufficiently small, namely below the order of the bare phonon frequency  $\omega_Q = \sqrt{4K/M}$ . It is thus set to be 0.2 fs except for the trivial crossings. Therefore, the solution of the time-dependent Schrödinger equation is finally written as [45]

$$\psi_{\mu}(t_{j+1}) = \sum_{\nu} \langle \varphi_{\nu} | \psi_{\mu}(t_j) \rangle \exp[-i\varepsilon_{\nu} \Delta t / \hbar] \varphi_{\nu}, \quad (10)$$

where  $\varphi_{\nu}$  and  $\varepsilon_{\nu}$  are the instantaneous eigenfunctions and eigenvalues of the Hamiltonian, respectively.

The eigenfunctions of the Hamiltonian can be expressed with the original diabatic orbitals,  $\varphi_{\nu} = \sum_n p_{n,\nu} |n\rangle$ . The electronic wavefunction is described with a linear expansion of these eigenfunctions,  $\psi = \sum_{\nu} c_{\nu} \varphi_{\nu}$ . The time-dependent Schrödinger equation is then written as

$$\dot{c}_{\nu} = \frac{1}{i\hbar} c_{\nu} \varepsilon_{\nu} - \sum_{\mu \neq \nu} c_{\mu} \sum_n \dot{u}_n d_{\nu,\mu}^n, \quad (11)$$

with  $d_{\nu,\mu}^n = \langle \varphi_{\nu} | d\varphi_{\mu}/du_n \rangle$  being the non-adiabatic coupling which is obtained by the Hellmann-Feynman theorem, i.e.,

$$d_{\nu,\mu}^n = \frac{\alpha_n [p_{n,\nu}(p_{n-1,\mu} - p_{n+1,\mu}) + p_{n,\mu}(p_{n-1,\nu} - p_{n+1,\nu})]}{\varepsilon_{\mu} - \varepsilon_{\nu}}. \quad (12)$$

If the quantumness of the system is strong enough, the charge injection will be dominated by the quantum tunneling which is featured by the non-adiabatic transitions among different PESs adhere to the electrode and organic molecules, respectively. In inorganic semiconductors, one can simply consider a scattering process through, for example, a triangle-shaped energy barrier to simulate this tunneling effect. In organic semiconductors, however, the electron is self-trapped and relatively localized such that it is not easy for the electron to hop across the barriers by their own kinetic energy, and the electron-phonon interactions normally serve as the main driving force to induce the quantum tunnelings. To this end, we have to adopt the Tully's standard SH algorithm to take this tunneling effect into the

simulations, and the hopping probability from the active surface  $\nu$  to another surface  $\mu$  is given by [28]

$$g_{\nu,\mu} = \Delta t \cdot \frac{2\text{Re}(c_\nu c_\mu^* \sum_n \dot{u}_n d_{\nu,\mu}^n)}{c_\nu^* c_\nu}. \quad (13)$$

If  $g_{\nu,\mu} < 0$ , it is reset to be zero. A uniform random number  $\zeta$  is generated and then a surface hop takes place if  $\sum_{X \neq \nu}^{\mu-1} g_{\nu,X} < \zeta \leq \sum_{X \neq \nu}^\mu g_{\nu,X}$ . A velocity adjustment is then made to conserve the total energy if  $\varepsilon_\mu - \varepsilon_\nu < \frac{M}{2} \sum_n \dot{u}_n^2$ , i.e.,

$$\dot{u}'_n = \dot{u}_n + d_{\nu,\mu}^n \frac{A}{B} \left[ \sqrt{1 + 2(\varepsilon_\nu - \varepsilon_\mu) \frac{B}{A^2}} - 1 \right], \quad (14)$$

where  $A = \sum_n M \dot{u}_n d_{\nu,\mu}^n$  and  $B = \sum_n M d_{\nu,\mu}^n \cdot d_{\nu,\mu}^n$ . It is noted that the hop cannot occur if  $\varepsilon_\nu < \varepsilon_\mu - A^2/2B$ .

It is known that the trivial crossings are very common in large systems involving many electronic states due to the rapid change with time of the non-adiabatic couplings [46, 47]. Adaptive time intervals [29, 47–49] and manual surface hops [47, 50] have been proven to be valid in SH simulations to deal with the trivial crossings. Considering the computational cost and the size of our model system, we first adjust  $\Delta t$  to be 0.02 fs for the calculation of the explicit hopping probabilities and then make manual hops if  $\Delta t$  is not small enough. For simplicity, we only consider the electron residing on top of Fermi surface that stochastically hops from the active PES to another in a time step. To obtain smooth averaged curves of the time-dependent injected charges, 100 realizations for each simulation are performed.

### III. RESULTS AND DISCUSSION

We first discuss the dynamical process of the injected charges in the organic molecules. By using the SH algorithm, we calculate the injected charge distribution  $\rho_n(t)$  and the corresponding electric field distribution  $E_n(t)$  in the organic molecules at different time points with interfacial width  $W = 20a_0$ , bias voltage  $V_0 = 5\text{V}$  and temperature  $T = 300\text{K}$ . As shown in Fig. 1(a), driven by the applied bias voltage, charges initially residing in the metallic electrode are injected into the organic molecules by overcoming the interfacial barrier induced by the Peierls instability and then quickly spread onto the whole organic molecules. Afterward, enforced by the built-in electric field  $E_n(t)$ , the injected charges are redistributed and accumulated on the left hand side of the organic molecules near the metal/organic interface after a relaxation time of  $\sim 80$  fs. This is because we do not consider the other



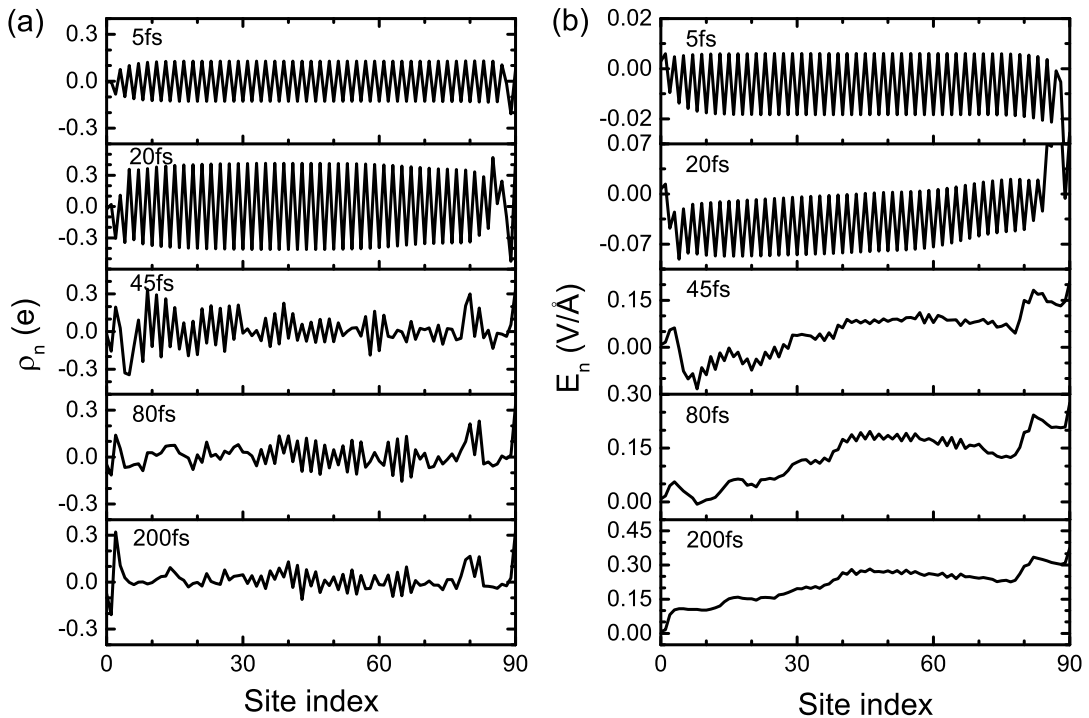


FIG. 1: (a) The injected charge distribution  $\rho_n(t)$  and (b) the corresponding electric field distribution  $E_n(t)$  in the organic molecules at different time points with  $W = 20a_0$ ,  $V_0 = 5$  V and  $T = 300$  K.

electrode in the devices such that there is not a drain for the carriers; we are dealing with a single contact for the first step. From Fig. 1(b), one can find that  $E_n(t)$  becomes larger with more charges being injected into the organic layer, which in turn further promotes the redistribution of the injected charges. It is known that the formation of stable localized polaron generally takes place in the charge injection process in the  $\pi$ -conjugated systems such as polyacetylene [23, 25, 26, 51]. However, it is also reported that the transport characteristics of molecular crystals, such as pentacene and rubrene, generally show high mobility and delocalized quantum carriers [52–55], which is quite different from that in the  $\pi$ -conjugated systems. Benefitting from the utilization of quantum dynamic approach combined with the Poisson’s equation, the phenomenon of the delocalization-localization transition of the injected charges in organic molecular materials under the applied bias voltage can be well simulated.

In order to show the crucial role of quantum tunneling in charge injection, we give a comparison of efficiency for the charge injection at the metal/organic interfaces by individ-

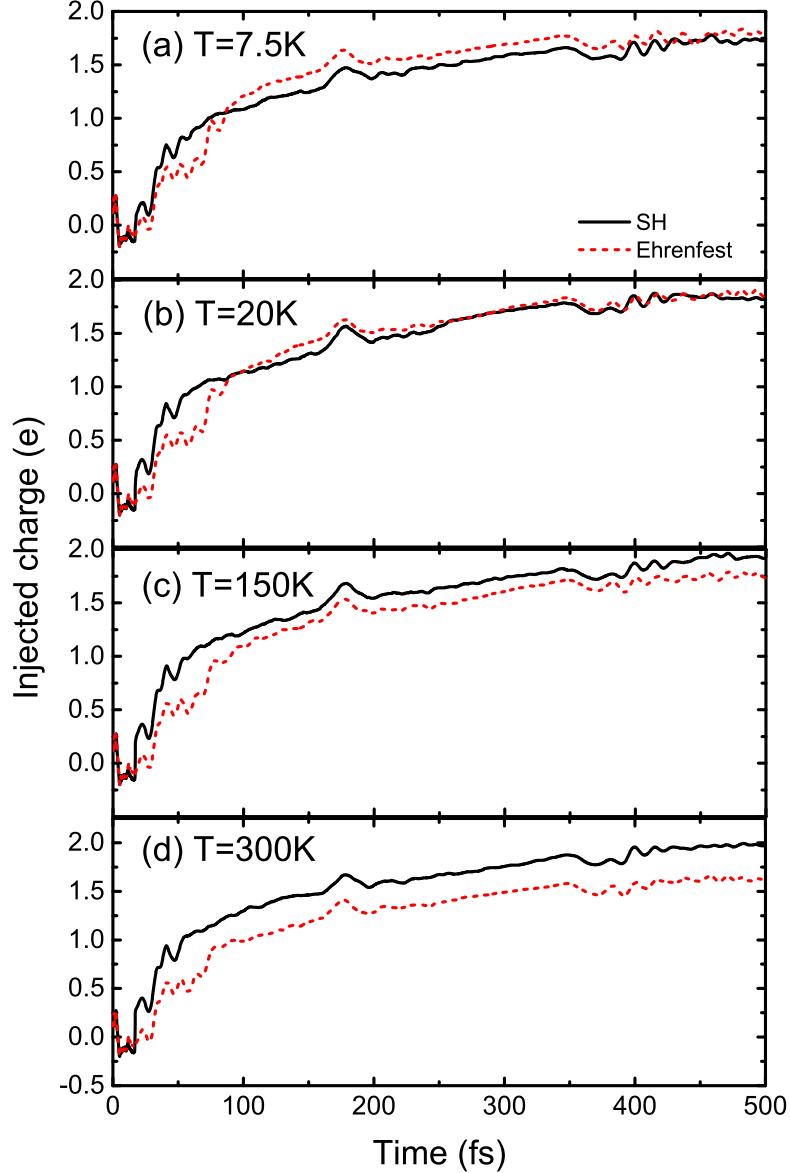


FIG. 2: Time evolution of the injected charge into the organic molecules for various temperatures  $T =$  (a) 7.5 K, (b) 20 K, (c) 150 K and (d) 300 K for the comparison between the SH algorithm and the Ehrenfest dynamics. The other parameters are:  $W = 20a_0$  and  $V_0 = 5$  V.

ually using the SH algorithm and the Ehrenfest dynamic approach. Fig. 2 displays the time evolution of the injected charges  $Q$  at four typical temperatures from low to high. The other parameters are  $W = 20a_0$  and  $V_0 = 5$  V. One can observe that  $Q$  increases gradually with evolution time and finally converges to different values at several hundreds of femtoseconds. The noticeable differences of the dynamic properties should be emphasized for these two methods. It can be found from Fig. 2(a) that,  $Q$  calculated by the Ehrenfest dynamics

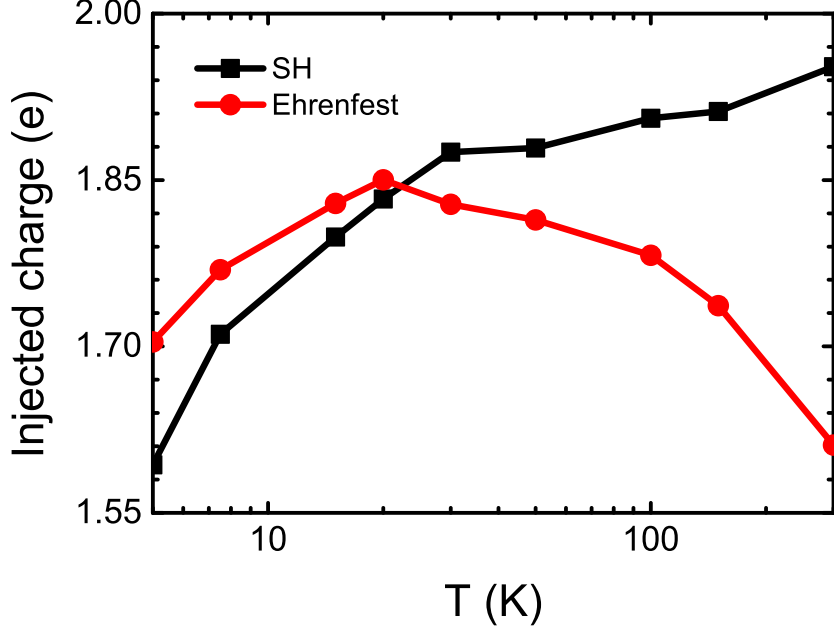


FIG. 3: Injected charge versus the temperature for the comparison between the SH algorithm and the Ehrenfest dynamics with  $W = 20a_0$  and  $V_0 = 5$  V.

is larger than that by the SH algorithm at ultralow temperature  $T = 7.5$  K. However, with temperature increasing,  $Q$  calculated by the SH algorithm becomes close to that of the Ehrenfest dynamics at  $T = 20$  K (see Fig. 2(b)) and then gets to be larger at  $T = 150$  K and  $T = 300$  K (see Fig. 2(c) and (d), respectively) due to the quantum tunneling represented by the non-adiabatic transition between PESs adhere to the electrode and organic molecules.

To further manifest the advantages of the SH algorithm for simulating the charge injection, we calculate the mean value of injected charges  $Q$  over the smooth time range between 400 fs and 500 fs for more typical temperatures. Fig. 3 shows the temperature dependence of  $Q$  obtained by the SH algorithm and the Ehrenfest dynamics with  $W = 20a_0$  and  $V_0 = 5$  V. The curves can be analyzed in two different temperature regimes. One is from 5 K to 30 K, in which  $Q$  obtained by the Ehrenfest dynamics is slightly larger than that from the SH algorithm, and the other is from 30 K to 300 K, in which  $Q$  obtained by the SH algorithm is significantly larger. More importantly, the temperature dependence of injected charges calculated from Ehrenfest dynamics shows a counterintuitive result that the charge injection efficiency decreases with increasing temperature, so we can conclude the Ehrenfest dynamics breaks down at room temperature. The reason is that, at low temperature the non-adiabatic transitions are largely suppressed so the mean-field treatment of PES in Ehrenfest dynamics

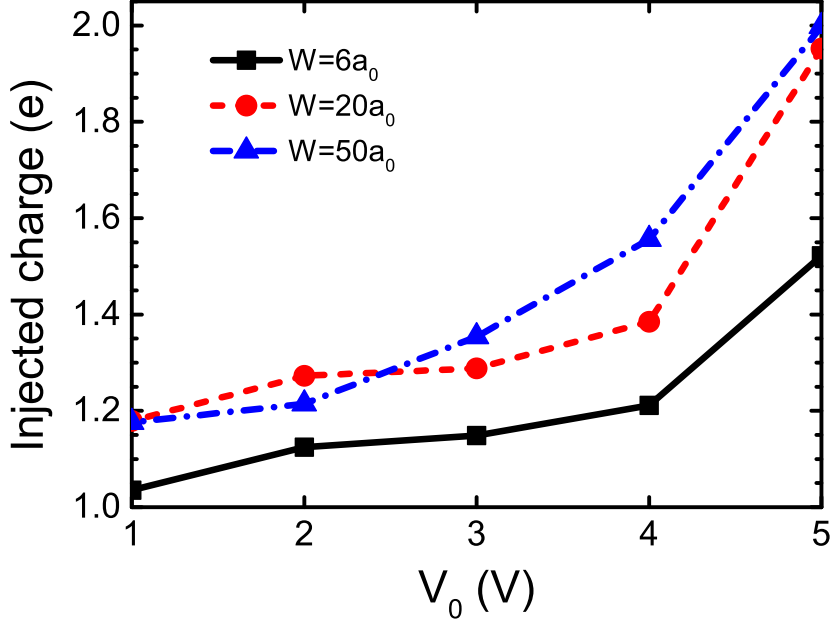


FIG. 4: Injected charge versus the applied bias voltage  $V_0$  by using the SH algorithm for various interfacial width  $W$  with  $T = 300$  K.

shares the similar results with the SH algorithm. At room temperature, on the other hand, non-adiabatic transitions obviously dominate the charge injection so we have to use SH algorithm to properly simulate this process. It is also found that the lineshape deviates from that of Richardson formula, namely  $\sim T^2 \exp(-\phi/k_B T)$  with  $\phi$  being the injection barrier. Our result exhibits larger injection efficiency than that from the Richardson formula within 30 K to 300 K, which is explicitly the consequence of involving quantum effects.

For the sake of device modeling, our dynamic approach has to be working with the influence of the bias voltage  $V_0$  applied at the metallic electrode on the charge injection efficiency. To this end, three different values of  $W$  are chosen for the calculation of the total injected charges at  $T = 300$  K, which is displayed in Fig. 4. It shows a monotonic increase of  $Q$  with the increase of  $V_0$  for three values of  $W$ . When a larger  $V_0$  is applied at the metallic electrode, the initial electric field in the organic layer becomes larger, which has a stronger promoting effect to the charge injection. Surprisingly, when the value of  $V_0$  is low to be 1 V which is about half of the bandgap of rubrene ( $\sim 2.2$  eV), the charges can still be injected into the organic molecules efficiently. In spite of the combined electric field simulation in our model, this result shows the low-threshold injection characteristics of these molecular crystals such as rubrene, which is quite in agreement with the experimental results [36–40].

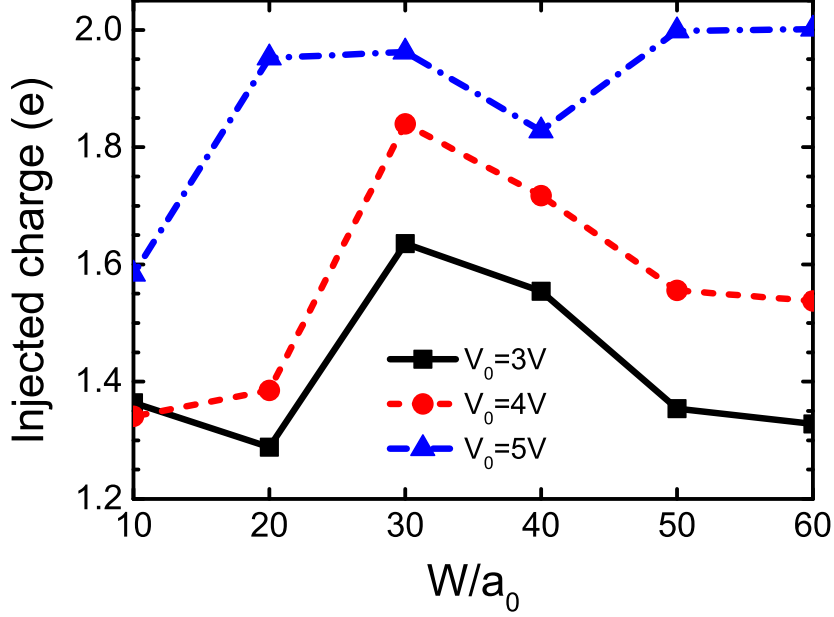


FIG. 5: Injected charge versus the interfacial width  $W$  by using the SH algorithm for various bias voltage  $V_0$  with  $T = 300$  K.

Moreover, from Fig. 4 one can also find that  $Q$  becomes larger when the larger  $W$  is applied in the range of high  $V_0$  while the trend is not obvious when  $V_0$  is lower than 3 V, implying the efficiency of charge injection at the metal/organic interfaces is closely related to the width of the interfacial layer which should be further investigated.

As well known, interfaces are essential for organic semiconductors in any way. In our previous work, we have discussed an optimum width of donor/acceptor (D/A) interface for the dissociation of the charge-transfer (CT) state [45]. In the practical fabrication of devices, the insertion of a buffer layer between the metallic electrode and the organic layer can effectively facilitate the injection of charge [56–59] and Hou’s group has obtained an optimal buffer layer width of several nanometers based on the model calculations and the experimental investigations [56]. Here with our dynamic approach, we can also determine an optimum width of the metal/organic interface for the charge injection. Fig. 5 displays the injected charges  $Q$  among various interfacial widths at certain  $V_0$  with  $T = 300$  K. For the cases of  $V_0 = 3$  V and  $V_0 = 4$  V, with the increase of the interfacial width,  $Q$  dramatically increases for  $W < 30a_0$  followed by a remarkable decrease. Differently, for the case of  $V_0 = 5$  V,  $Q$  first dramatically increases and then behaves a slight increase except for the case  $W = 40a_0$ . As a consequence here, the optimum value of the interfacial width

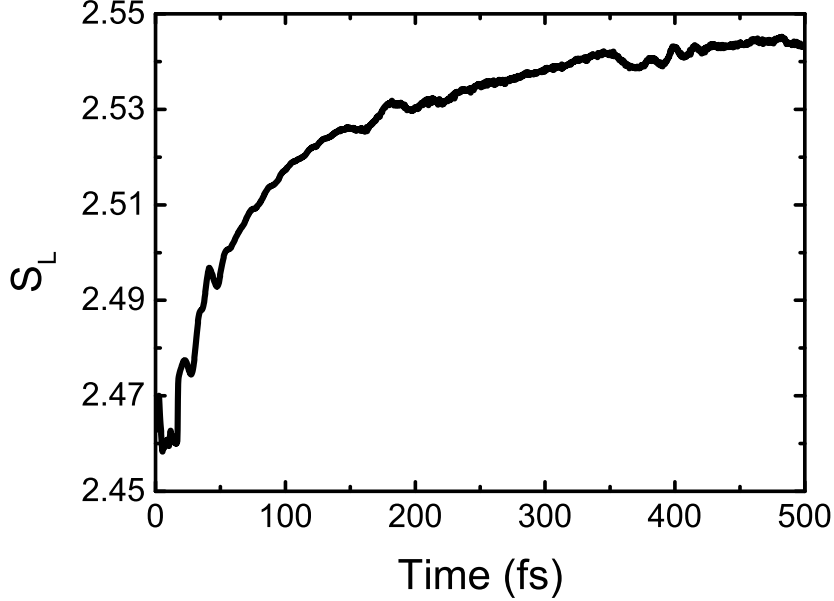


FIG. 6: Time evolution of the von Neumann entropy  $S_L$  of the injected charges with  $W = 20a_0$ ,  $V_0 = 5$  V and  $T = 300$  K.

for the charge injection is determined to be  $30a_0$  ( $\sim 10$  nm) in our case, which is consistent with Hou's results [56].

Before ending this section, we would like to discuss more on the quantumness of the charge injection process at the metal/organic interfaces. As stated above, the classical thermionic emission theory can not be directly applied to the organic semiconductors; lots of quantum effects have been discussed in this systems especially taking photoemission into consideration [17, 18, 60]. To this end, we calculate the von Neumann entropy of the injected charges, which is defined as [61, 62]:

$$S_L = -\text{Tr}(\rho_L \ln \rho_L), \quad (15)$$

where  $\rho_L$  is the reduced density matrix of the charges in organic molecules. Fig. 6 exhibits the time evolution of the von Neumann entropy  $S_L$  of the system in the charge injection process with  $W = 20a_0$ ,  $V_0 = 5$  V and  $T = 300$  K. It is found that  $S_L$  increases gradually with evolution time and finally saturates to a constant. We notice that, the total increase of entropy is roughly by 3%, not significant compared with our expectation as we expected that following more charges are injected the entropy would largely increases making the quantumness quickly lost. In our previous work, we have also present a coherent scenario of the dissociation of the CT state at the D/A interfaces in the organic photovoltaics [45].

Combined these two studies, our findings may enlighten the understanding of the quantumness of charge dynamics in organic semiconductors which may facilitate the establishment of a systematic device modeling method specifically for this system.

#### IV. CONCLUSION AND OUTLOOK

In summary, we develop a unified dynamic approach based upon surface hopping algorithm combined with Poisson's equation to investigate the charge injection process at metal/organic interface. It is found that the charges can be dynamically injected into the organic materials and then quickly spread onto the molecules in a delocalized fashion followed by an accumulation induced by the built-in electric field. The injected charges obtained by the SH algorithm are compared with that by the Ehrenfest dynamics, and the former one works well for simulating efficient charge injection at room temperature while the latter one is merely valid at ultralow temperature. The influence of the bias voltage applied at the metallic electrode on the charge injection efficiency is discussed and the injected charges behave a significant increase by increasing applied bias voltage. With the assistance of quantum effect, the charges could be injected into the organic molecules efficiently even if the bias voltage is small compared with the bandgap of the organic material, which can be utilized to explain the low-threshold feature. The width of  $\sim 10$  nm is regarded to be the optimum value of the interfacial layer for the charge injection at the metal/organic interfaces. In addition, the von Neumann entropy provides a further insight into the quantumness of the charge injection dynamics.

In inorganic semiconductors the thermal equilibrium is basically valid in an approximate manner, since the thermal motions of atoms are almost completely disordered. In contrast, the molecular vibrations in organic materials are always concentrated at some specific modes so that the quantum coherence of electrons could be well protected to keep quantumness alive. In organic photovoltaic devices, the coherent exciton dynamics has been demonstrated in many experiments and widely discussed [63–66]. As the majority charge carriers in organic semiconductors stem from injection at the interfaces other than doping, the normal thermionic emission theory is not sufficient for us to understand the conductivity in these devices. A dynamic scenario serves as an alternative perspective. With this unified dynamic approach in hand, we can in the future establish a systematic device modeling method

to mimic the device performance giving the material parameters obtained from quantum chemistry computations. We believe this first-principle framework could help us simulate the organic semiconducting devices in a more appropriate and efficient way.

## ACKNOWLEDGMENTS

The authors gratefully acknowledge support from the National Natural Science Foundation of China (Grant No. 91833305 and 11974118), the Key R&D Project of Guangdong Province (Grant No. 2020B0303300001) and the Fundamental Research Funds for the Central Universities (Grant No. 2019ZD51).

- 
- [1] F. Huang, H. Wu, and Y. Cao, Water/alcohol soluble conjugated polymers as highly efficient electron transporting/injection layer in optoelectronic devices, *Chem. Soc. Rev.* **39**, 2500 (2010).
  - [2] Q. Wang, Y. Zhou, H. Zheng, J. Shi, C. Li, C. Q. Su, L. Wang, C. Luo, D. Hu, J. Pei, J. Wang, J. Peng, and Y. Cao, Modifying organic/metal interface via solvent treatment to improve electron injection in organic light emitting diodes, *Org. Electron.* **12**, 1858 (2011).
  - [3] B. R. Lee, J.-w. Kim, D. Kang, D. W. Lee, S.-J. Ko, H. J. Lee, C.-L. Lee, J. Y. Kim, H. S. Shin, and M. H. Song, Highly efficient polymer light-emitting diodes using graphene oxide as a hole transport layer, *ACS Nano* **6**, 2984 (2012).
  - [4] Z. Zhong, Z. Hu, Z. Jiang, J. Wang, Y. Chen, C. Song, S. Han, F. Huang, J. Peng, J. Wang, and Y. Cao, Hole-Trapping Effect of the Aliphatic-Amine Based Electron Injection Materials in the Operation of OLEDs to Facilitate the Electron Injection, *Adv. Electron. Mater.* **1**, 1400014 (2015).
  - [5] Z. Hu, Z. Zhong, K. Zhang, Z. Hu, C. Song, F. Huang, J. Peng, J. Wang, and Y. Cao, Dipole formation at organic/metal interfaces with pre-deposited and post-deposited metal, *NPG Asia Mater.* **9**, e379 (2017).
  - [6] S. M. Sze, *Physics of Semiconductor Devices* (Wiley, New York, 1981).
  - [7] N. Koch and A. Vollmer, Electrode-molecular semiconductor contacts: Work-function-dependent hole injection barriers versus Fermi-level pinning, *Appl. Phys. Lett.* **89**, 162107



- (2006).
- [8] W. Osikowicz, M. P. de Jong, S. Braun, C. Tengstedt, M. Fahlman, and W. R. Salaneck, Energetics at Au top and bottom contacts on conjugated polymers, *Appl. Phys. Lett.* **88**, 193504 (2006).
  - [9] C. Tengstedt, W. Osikowicz, W. R. Salaneck, I. D. Parker, C.-H. Hsu, and M. Fahlman, Fermi-level pinning at conjugated polymer interfaces, *Appl. Phys. Lett.* **88**, 053502 (2006).
  - [10] A. Crispin, X. Crispin, M. Fahlman, M. Berggren, and W. R. Salaneck, Transition between energy level alignment regimes at a low band gap polymer-electrode interfaces, *Appl. Phys. Lett.* **89**, 213503 (2006).
  - [11] K. Stokbro and S. Smidstrup, Electron transport across a metal-organic interface: Simulations using nonequilibrium Green's function and density functional theory, *Phys. Rev. B* **88**, 075317 (2013).
  - [12] A. Troisi and G. Orlandi, Charge-transport regime of crystalline organic semiconductors: diffusion limited by thermal off-diagonal electronic disorder, *Phys. Rev. Lett.* **96**, 086601 (2006).
  - [13] A. Troisi, Prediction of the Absolute Charge Mobility of Molecular Semiconductors: the Case of Rubrene, *Adv. Mater.* **19**, 2000 (2007).
  - [14] L. Wang, D. Beljonne, L. Chen, and Q. Shi, Mixed quantum-classical simulations of charge transport in organic materials: Numerical benchmark of the Su-Schrieffer-Heeger model, *J. Chem. Phys.* **134**, 244116 (2011).
  - [15] L. Wang, A. V. Akimov, L. Chen, and O. V. Prezhdo, Quantized Hamiltonian dynamics captures the low-temperature regime of charge transport in molecular crystals, *J. Chem. Phys.* **139**, 174109 (2013).
  - [16] L. Wang and D. Beljonne, Charge transport in organic semiconductors: Assessment of the mean field theory in the hopping regime, *J. Chem. Phys.* **139**, 064316 (2013).
  - [17] M. Barbatti, Nonadiabatic dynamics with trajectory surface hopping method, *WIREs Comput. Mol. Sci.* **1**, 620 (2011).
  - [18] J. E. Subotnik, A. Jain, B. Landry, A. Petit, W. Ouyang, and N. Bellonzi, Understanding the Surface Hopping View of Electronic Transitions and Decoherence, *Annu. Rev. Phys. Chem.* **67**, 387 (2016).
  - [19] J. C. Tully, Perspective: Nonadiabatic dynamics theory, *J. Chem. Phys.* **137**, 22A301 (2012).

- [20] L. Wang, O. V. Prezhdo, and D. Beljonne, Mixed quantum-classical dynamics for charge transport in organics, *Phys. Chem. Chem. Phys.* **17**, 12395 (2015).
- [21] L. Wang, A. Akimov, and O. V. Prezhdo, Recent Progress in Surface Hopping: 2011-2015, *J. Phys. Chem. Lett.* **7**, 2100 (2016).
- [22] L. Wang, J. Qiu, X. Bai, and J. Xu, Surface hopping methods for nonadiabatic dynamics in extended systems, *WIREs Comput. Mol. Sci.* **10**, e1435 (2019).
- [23] C. Q. Wu, Y. Qiu, Z. An, and K. Nasu, Dynamical study on polaron formation in a metal/polymer/metal structure, *Phys. Rev. B* **68**, 125416 (2003).
- [24] Y. H. Yan, Z. An, C. Q. Wu, and K. Nasu, Formation dynamics of bipolaron in a metal/polymer/metal structure, *Eur. Phys. J. B* **48**, 501 (2005).
- [25] A. A. Johansson and S. Stafström, Nonadiabatic simulations of polaron dynamics, *Phys. Rev. B* **69**, 235205 (2004).
- [26] J.-y. Fu, J.-f. Ren, X.-j. Liu, D.-s. Liu, and S.-j. Xie, Dynamics of charge injection into an open conjugated polymer: A nonadiabatic approach, *Phys. Rev. B* **73**, 195401 (2006).
- [27] L. A. Ribeiro Junior and W. F. da Cunha, Nonadiabatic dynamics of injected holes in conjugated polymers, *Phys. Chem. Chem. Phys.* **19**, 10000 (2017).
- [28] J. C. Tully, Molecular dynamics with electronic transitions, *J. Chem. Phys.* **93**, 1061 (1990).
- [29] L. Wang and D. Beljonne, Flexible Surface Hopping Approach to Model the Crossover from Hopping to Band-like Transport in Organic Crystals, *J. Phys. Chem. Lett.* **4**, 1888 (2013).
- [30] L. Wang and O. V. Prezhdo, A Simple Solution to the Trivial Crossing Problem in Surface Hopping, *J. Phys. Chem. Lett.* **5**, 713 (2014).
- [31] L. Wang, D. Trivedi, and O. V. Prezhdo, Global Flux Surface Hopping Approach for Mixed Quantum-Classical Dynamics, *J. Chem. Theory Comput.* **10**, 3598 (2014).
- [32] A. E. Sifain, L. Wang, and O. V. Prezhdo, Mixed quantum-classical equilibrium in global flux surface hopping, *J. Chem. Phys.* **142**, 224102 (2015).
- [33] J. Qiu, X. Bai, and L. Wang, Crossing Classified and Corrected Fewest Switches Surface Hopping, *J. Phys. Chem. Lett.* **9**, 4319 (2018).
- [34] J. Qiu, X. Bai, and L. Wang, Subspace Surface Hopping with Size-Independent Dynamics, *J. Phys. Chem. Lett.* **10**, 637 (2019).
- [35] X. Bai, J. Qiu, and L. Wang, An efficient solution to the decoherence enhanced trivial crossing problem in surface hopping, *J. Chem. Phys.* **148**, 104106 (2018).

- [36] A. K. Pandey and J.-M. Nunzi, Upconversion injection in rubrene/perylene-diimide heterostructure electroluminescent diodes, *Appl. Phys. Lett.* **90**, 263508 (2007).
- [37] A. K. Pandey and J. M. Nunzi, Rubrene/Fullerene Heterostructures with a Half-Gap Electroluminescence Threshold and Large Photovoltage, *Adv. Mater.* **19**, 3613 (2007).
- [38] C. Xiang, C. Peng, Y. Chen, and F. So, Origin of Sub-Bandgap Electroluminescence in Organic Light-Emitting Diodes, *Small* **11**, 5439 (2015).
- [39] Q. Chen, W. Jia, L. Chen, D. Yuan, Y. Zou, and Z. Xiong, Determining the Origin of Half-bandgap-voltage Electroluminescence in Bifunctional Rubrene/C60 Devices, *Sci. Rep.* **6**, 25331 (2016).
- [40] S.-J. He and Z.-H. Lu, Ultralow-voltage Auger-electron-stimulated organic light-emitting diodes, *J. Photon. Energy* **6**, 036001 (2016).
- [41] C. Pflumm, C. Gärtner, and U. Lemmer, A numerical scheme to model current and voltage excitation of organic light-emitting diodes, *IEEE J. Quantum Electron.* **44**, 790 (2008).
- [42] N. S. Christ, S. W. Kettlitz, S. Valouch, S. Züfle, C. Gärtner, M. Punke, and U. Lemmer, Nanosecond response of organic solar cells and photodetectors, *J. Appl. Phys.* **105**, 104513 (2009).
- [43] D. Li, L. Song, Y. Chen, and W. Huang, Modeling Thin Film Solar Cells: From Organic to Perovskite, *Adv. Sci.* **7**, 1901397 (2020).
- [44] V. I. Arkhipov and H. Bässler, Exciton dissociation and charge photogeneration in pristine and doped conjugated polymers, *Phys. Status Solidi A* **201**, 1152 (2004).
- [45] J. Huang, Y. Mo, and Y. Yao, Charge-transfer state dynamics in all-polymer solar cells: formation, dissociation and decoherence, *Phys. Chem. Chem. Phys.* **21**, 2755 (2019).
- [46] G. Granucci, M. Persico, and A. Toniolo, Direct semiclassical simulation of photochemical processes with semiempirical wave functions, *J. Chem. Phys.* **114**, 10608 (2001).
- [47] S. Fernandez-Alberti, A. E. Roitberg, T. Nelson, and S. Tretiak, Identification of unavoided crossings in nonadiabatic photoexcited dynamics involving multiple electronic states in polyatomic conjugated molecules, *J. Chem. Phys.* **137**, 014512 (2012).
- [48] A. M. Virshup, B. G. Levine, and T. J. Martinez, Steric and electrostatic effects on photoisomerization dynamics using QM/MM ab initio multiple spawning, *Theor. Chem. Acc.* **133**, 1506 (2014).
- [49] L. Spörkel and W. Thiel, Adaptive time steps in trajectory surface hopping simulations, *J.*

- Chem. Phys. **144**, 194108 (2016).
- [50] E. Fabiano, T. W. Keal, and W. Thiel, Implementation of surface hopping molecular dynamics using semiempirical methods, Chem. Phys. **349**, 334 (2008).
- [51] S. V. Rakhmanova and E. M. Conwell, Polaron dissociation in conducting polymers by high electric fields, Appl. Phys. Lett. **75**, 1518 (1999).
- [52] V. Podzorov, E. Menard, J. A. Rogers, and M. E. Gershenson, Hall effect in the accumulation layers on the surface of organic semiconductors, Phys. Rev. Lett. **95**, 226601 (2005).
- [53] O. Ostroverkhova, D. G. Cooke, F. A. Hegmann, J. E. Anthony, V. Podzorov, M. E. Gershenson, O. D. Jurchescu, and T. T. M. Palstra, Ultrafast carrier dynamics in pentacene, functionalized pentacene, tetracene, and rubrene single crystals, Appl. Phys. Lett. **88**, 162101 (2006).
- [54] T. Minari, T. Nemoto, and S. Isoda, Temperature and electric-field dependence of the mobility of a single-grain pentacene field-effect transistor, J. Appl. Phys. **99**, 034506 (2006).
- [55] M. E. Gershenson, V. Podzorov, and A. F. Morpurgo, Colloquium: Electronic transport in single-crystal organic transistors, Rev. Mod. Phys. **78**, 973 (2006).
- [56] S. T. Zhang, X. M. Ding, J. M. Zhao, H. Z. Shi, J. He, Z. H. Xiong, H. J. Ding, E. G. Obbard, Y. Q. Zhan, W. Huang, and X. Y. Hou, Buffer-layer-induced barrier reduction: Role of tunneling in organic light-emitting devices, Appl. Phys. Lett. **84**, 425 (2004).
- [57] T.-F. Guo, F.-S. Yang, Z.-J. Tsai, T.-C. Wen, S.-N. Hsieh, Y.-S. Fu, and C.-T. Chung, Organic oxide/Al composite cathode in efficient polymer light-emitting diodes, Appl. Phys. Lett. **88**, 113501 (2006).
- [58] T.-F. Guo, F.-S. Yang, Z.-J. Tsai, T.-C. Wen, C.-I. Wu, and C.-T. Chung, Organic oxide/Al composite cathode in small molecular organic light-emitting diodes, Appl. Phys. Lett. **89**, 053507 (2006).
- [59] T.-H. Lee, J.-C.-A. Huang, G. L. v. Pakhomov, T.-F. Guo, T.-C. Wen, Y.-S. Huang, C.-C. Tsou, C.-T. Chung, Y.-C. Lin, and Y.-J. Hsu, Organic-Oxide Cathode Buffer Layer in Fabricating High-Performance Polymer Light-Emitting Diodes, Adv. Funct. Mater. **18**, 3036 (2008).
- [60] T. Nelson, S. Fernandez-Alberti, A. E. Roitberg, and S. Tretiak, Nonadiabatic excited-state molecular dynamics: modeling photophysics in organic conjugated materials, Acc. Chem. Res. **47**, 1155 (2014).

- [61] A. M. Läuchli and C. Kollath, Spreading of correlations and entanglement after a quench in the one-dimensional Bose-Hubbard model, *J. Stat. Mech.* P05018 (2008).
- [62] L. Amico, R. Fazio, A. Osterloh, and V. Vedral, Entanglement in many-body systems, *Rev. Mod. Phys.* **80**, 517 (2008).
- [63] S. M. Falke, C. A. Rozzi, D. Brida, M. Maiuri, M. Amato, E. Sommer, A. De Sio, A. Rubio, G. Cerullo, E. Molinari, and C. Lienau, Coherent ultrafast charge transfer in an organic photovoltaic blend, *Science* **344**, 1001 (2014).
- [64] Y. Song, S. N. Clifton, R. D. Pensack, T. W. Kee, and G. D. Scholes, Vibrational coherence probes the mechanism of ultrafast electron transfer in polymer-fullerene blends, *Nat. Commun.* **5**, 4933 (2014).
- [65] Y. Song, C. Hellmann, N. Stingelin, and G. D. Scholes, The separation of vibrational coherence from ground- and excited-electronic states in P3HT film, *J. Chem. Phys.* **142**, 212410 (2015).
- [66] A. De Sio, F. Troiani, M. Maiuri, J. Rehault, E. Sommer, J. Lim, S. F. Huelga, M. B. Plenio, C. A. Rozzi, G. Cerullo, E. Molinari, and C. Lienau, Tracking the coherent generation of polaron pairs in conjugated polymers, *Nat. Commun.* **7**, 13742 (2016).